Compact Conversion and Cyclostationary Noise Modeling of pn–Junction Diodes in Low-Injection—Part I: Model Derivation

Fabrizio Bonani, *Senior Member, IEEE*, Simona Donati Guerrieri, *Member, IEEE*, and Giovanni Ghione, *Senior Member, IEEE*

***Abstract*—Starting from the well known low-injection approximation, a closed form, analytical compact model is derived for the small-signal (SS) and forced quasi-periodic operation of junction diodes. The model determines the small-signal and conversion admittance matrix of the device as a function of the applied (dc or periodic-time varying) bias. Noise characteristics, in both the stationary (SS) and cyclostationary cases, are also evaluated by means of a Green's function approach.**

***Index Terms*—Frequency conversion, pn–junctions, semiconductor device modeling, semiconductor device noise.**

I. Introduction

THE DC, ac and small-signal noise modeling of pn–junction diodes is a classical, well established topic in electron device design. The dc diode theory in low-injection conditions was proposed in the 1940s–1950s (see [1] and references therein); in the same period, a small-signal distributed diode ac model was then developed through the solution of the frequency-domain continuity equations in the quasineutral diode sides [1]. Concerning small-signal noise modeling, a complete physics-based analysis based on Green's function techniques was developed by Van Vliet in [2], although the empirical (but, as pointed out already by van der Ziel [3], widely misinterpreted) shot-noise model had been widely used for years in circuit design. Further extensions in the field of diode modeling was stimulated by radio frequency (RF) applications in which junction diodes were exploited to perform frequency conversion (like in resistive mixers and frequency multipliers). Starting from the pioneering paper by Dragone [4] circuit-oriented models were developed for the so-called small-signal large-signal (SSLS) or conversion diode behavior [5] and for the cyclostationary diode noise arising under large-signal periodic excitation. While the conversion matrix diode model proved successful in circuit design, a number of basic issues involving noise modulation and conversion are still a matter of active research [6], [7].

Manuscript received July 29, 2003. This work was supported in part by the Center of Excellence for Multimedia Radiocommunications (CERCOM) of Politecnico di Torino. The review of this paper was arranged by Editor M. J. Deen.

F. Bonani and G. Ghione are with INFM Unità Torino Politecnico, Politecnico di Torino, 10129 Torino, Italy, and also with the Dipartimento di Elettronica, Politecnico di Torino, 10129 Torino, Italy.

S. Donati Guerrieri is with the Dipartimento di Elettronica, Politecnico di Torino, 10129 Torino, Italy.

Digital Object Identifier 10.1109/TED.2003.821570

Although numerical physics-based semiconductor device simulation, recently extended to the large-signal noise and conversion modeling [8]–[10], has provided during the last few years a valuable tool for device design, closed-form, computationally efficient models (often referred to as compact models) still are a valuable asset, and often an indispensable tool in circuit design. In the present paper we propose a closed-form analytical distributed model for frequency conversion and cyclostationary noise for pn–junction diodes in low-injection conditions, providing the diode conversion matrix and noise sideband correlation matrix [11]. For conversion modeling, the approach can be considered as a straightforward extension and generalization of the small-signal distributed model based on the analytical solution of the diffusion equations in the quasineutral diode sides, while the cyclostationary noise model extends the small-signal Green's function approach [12]. The model validation through comparisons with results from numerical models is presented in the companion paper [13], together with a further discussion on circuit-oriented compact model strategies for cyclostationary noise modeling. Furthermore, besides its practical interest per se in RF and microwave analog applications, the present compact model is also the basis for conversion and cyclostationary noise modeling in other junction devices, such as the bipolar transistor.

The structure considered in the derivation of the model, shown in Fig. 1, is an abrupt one-dimensional (1-D) junction, with constant doping in the two sides. The depletion region width is $x_n + x_p$, and the two neutral regions have widths $w_n - x_n$ and $w_p - x_p$ in the n and p sides, respectively.

The compact diode model is based on the standard low-injection theory expressing the junction (intrinsic) current as the sum of minority carrier diffusion currents in the two quasineutral sides of the device, thus neglecting the current contribution due to generation-recombination (GR) in the depletion region [14]; majority carrier densities are approximated by their equilibrium value. Furthermore, the parasitic resistance R_s, associated to the resistivity of the neutral regions, and the junction depletion capacitance C_j have to be included in the model according to the circuit in Fig. 2, where the junction voltage v_j and current i are defined, as well as the applied device voltage v_a and current i_a. By extending the customary terminology for transistors, the junction variables will also be called intrinsic.

The paper is structured as follows: In Section II the basic equations for the derivation of the diode compact model are introduced, including the relevant boundary conditions. Sec-

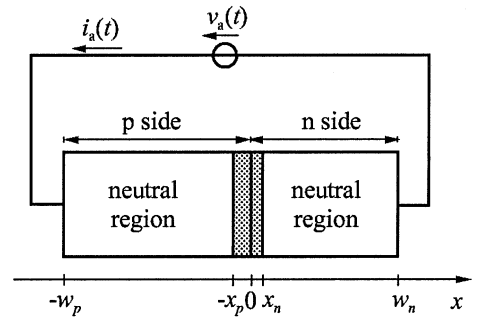

Fig. 1. Structure of the pn–junction diode.

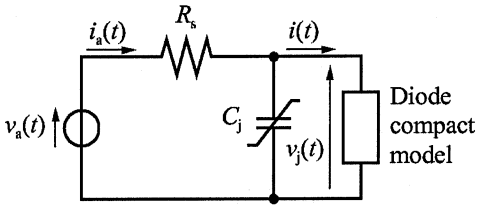

Fig. 2. Equivalent circuit of the pn–junction diode.

tion III is devoted to the evaluation of the small-signal diode admittance and of the large-signal admittance conversion matrix. The small-signal and cyclostationary noise compact models are derived in Sections IV and V, respectively. Finally, conclusions are drawn in Section VI.

II. Basic Equations

This section is devoted to the discussion of the basic equations used in deriving the compact model. We separately consider the evaluation of the device working point (dc or periodically time-varying) in Section II-A, the perturbation approach to small-signal (SS) and conversion (see [5] and [8] for an introduction) analyzes in Section II-B, and the noise model in Section II-C.

A. Working Point

Let us consider first the evaluation of the device working point; the related variables will be denoted throughout the paper by subscript "0." The working point is set by the applied voltage $v_{a0}(t)$, determining the intrinsic working point voltage $v_{j0}(t)$. Two cases are considered: dc operation, wherein v_{j0} is independent of time, and periodic large-signal (LS) conditions, corresponding to a a periodically time-varying working point with fundamental (angular) frequency ω_0.

In both cases, according to the device structure in Fig. 1, the low-injection device current is written as

$$i = qAD_n \frac{\partial n'_p}{\partial x}\bigg|_{x=-x_p} - qAD_p \frac{\partial p'_n}{\partial x}\bigg|_{x=x_n} \tag{1}$$

where q is the electron charge, A is the cross section, D is the minority carrier diffusivity, $n'_p = n_p - n_{p,\mathrm{eq}}$ and $p'_n = p_n - p_{n,\mathrm{eq}}$ are the excess minority carrier densities, $n_{p,\mathrm{eq}} = n_i^2/N_A$ and $p_{n,\mathrm{eq}} = n_i^2/N_D$ are the equilibrium minority carrier densities, n_i is the intrinsic carrier concentration and N_A, N_D are the doping densities of the p and n side, respectively.

Neglecting the electric field in the quasineutral regions, the minority carrier continuity equations are expressed as

$$\frac{\partial n'_p}{\partial t} = -\frac{n'_p}{\tau_n} + D_n \frac{\partial^2 n'_p}{\partial x^2} \tag{2a}$$

$$\frac{\partial p'_n}{\partial t} = -\frac{p'_n}{\tau_p} + D_p \frac{\partial^2 p'_n}{\partial x^2} \tag{2b}$$

where τ is the minority carrier lifetime. The boundary conditions associated to (2) assume ohmic contacts at the device terminals

$$n'_p(-w_p, t) = 0, \qquad p'_n(w_n, t) = 0. \tag{3}$$

At the interface between depletion and neutral regions, the excess minority carrier concentration is related to the intrinsic voltage v_j through the junction law

$$n'_p(-x_p) = n_{p,\mathrm{eq}} \left[\exp\left(\frac{v_j}{V_T}\right) - 1\right] \tag{4a}$$

$$p'_n(x_n) = p_{n,\mathrm{eq}} \left[\exp\left(\frac{v_j}{V_T}\right) - 1\right] \tag{4b}$$

where $V_T = k_B T/q$, k_B is the Boltzmann constant and T is the temperature.

In dc conditions ($v_j(t) = v_{j0}$ independent of time), the solution of (2) is [14]

$$n'_{p0}(x) = n'_{p0}(-x_p) \frac{\sinh \frac{w_p + x}{L_n}}{\sinh \frac{w_p - x_p}{L_n}} \tag{5a}$$

$$p'_{n0}(x) = p'_{n0}(x_n) \frac{\sinh \frac{w_n - x}{L_p}}{\sinh \frac{w_n - x_n}{L_p}} \tag{5b}$$

where $L_\alpha = \sqrt{D_\alpha \tau_\alpha}$ is the diffusion length for carrier $\alpha = n, p$, and $n'_{p0}(-x_p)$ and $p'_{n0}(x_n)$ are given by (4) evaluated for $v_j(t) = v_{j0}$.

In LS operation, the periodically time-varying working point [5], [8] is expressed according to the Fourier decomposition

$$v_{j0}(t) = \sum_l (\tilde{v}_{j0})_l \exp(j\omega_l t) \tag{6}$$

where $(\tilde{v}_{j0})_l$ is the l-th harmonic component of signal $v_{j0}(t)$, at $\omega_l = l\omega_0$. The steady-state excess carrier concentrations are also a periodic function of time; thus

$$n'_{p0}(x,t) = \sum_l \left(\tilde{n}'_{p0}(x)\right)_l \exp(j\omega_l t) \tag{7}$$

with a similar expression for holes. Due to linearity of (2) and (3), (5) can be generalized into

$$\left(\tilde{n}'_{p0}(x)\right)_l = \left(\tilde{n}'_{p0}(-x_p)\right)_l \frac{\sinh \frac{w_p + x}{\tilde{L}_{n,l}}}{\sinh \frac{w_p - x_p}{\tilde{L}_{n,l}}} \tag{8a}$$

$$\left(\tilde{p}'_{n0}(x)\right)_l = \left(\tilde{p}'_{n0}(x_n)\right)_l \frac{\sinh \frac{w_n - x}{\tilde{L}_{p,l}}}{\sinh \frac{w_n - x_n}{\tilde{L}_{p,l}}} \tag{8b}$$

where $\tilde{L}_{\alpha,l} = L_\alpha/(a_{\alpha,l} + jb_{\alpha,l})$, $a_{\alpha,l} + jb_{\alpha,l} = \sqrt{1 + j\omega_l \tau_\alpha}$, and $\left(\tilde{n}'_{p0}(-x_p)\right)_l$ and $\left(\tilde{p}'_{n0}(x_n)\right)_l$ are the l-th harmonic components of the corresponding excess carrier densities, evaluated

by decomposing in Fourier series the junction law (4) with $v_j(t)$ given by (6).

Notice that the continuity equations (2) are, for constant mobility and diffusivity, linear, as well as the current expression (1). Therefore, according to the discussion in [15], the intrinsic diode can be modeled as the cascade of a nonlinear, memoryless system, corresponding to (4), and of a linear, time-invariant system represented by (1) and (2).

B. Perturbation Analysis

The small-signal (SS), conversion, and noise [12] analyzes are all based on a perturbation approach: the device (electrical and physical) variables are approximated as the sum of the working point-dependent part, and of a small perturbation, derived by linearizing the device equations around the working point. Since (1) and (2) are already linear, linearization must be performed on the boundary conditions (4) only.

Let us consider first the case of a dc working point, relevant to SS and stationary (small-signal) noise analyzes. The intrinsic voltage is decomposed as $v_j(t) = v_{j0} + \tilde{v}_j \exp(j\omega_{\rm SS}t)$, where v_{j0} is constant and an harmonic perturbation at (angular) frequency $\omega_{\rm SS}$ has been considered. This causes a perturbation of the excess minority carrier concentrations, having, in the limit of the small-change approximation, a harmonic time dependence at the same frequency: $n'_p(x,t) = n'_{p0}(x) + \tilde{n}'_p(x)\exp(j\omega_{\rm SS}t)$, with a similar expression for holes. From (2), the harmonic perturbations of the excess minority concentrations satisfy

$$j\omega_{\rm SS}\tilde{n}'_p = -\frac{\tilde{n}'_p}{\tau_n} + D_n\frac{d^2\tilde{n}'_p}{dx^2} \tag{9a}$$

$$j\omega_{\rm SS}\tilde{p}'_n = -\frac{\tilde{p}'_n}{\tau_p} + D_p\frac{d^2\tilde{p}'_n}{dx^2} \tag{9b}$$

whose boundary conditions are derived from (3)

$$\tilde{n}'_p(-w_p) = 0, \qquad \tilde{p}'_n(w_n) = 0 \tag{10}$$

and by linearizing (4) around v_{j0}

$$\tilde{n}'_p(-x_p) = n_{p,\rm eq}\exp\left(\frac{v_{j0}}{V_T}\right)\frac{\tilde{v}_j}{V_T} \tag{11a}$$

$$\tilde{p}'_n(x_n) = p_{n,\rm eq}\exp\left(\frac{v_{j0}}{V_T}\right)\frac{\tilde{v}_j}{V_T}. \tag{11b}$$

The (harmonic) perturbation of the intrinsic current is evaluated starting from (1)

$$\tilde{\imath} = qAD_n\frac{d\tilde{n}'_p}{dx}\bigg|_{x=-xp} - qAD_p\frac{d\tilde{p}'_n}{dx}\bigg|_{x=x_n}. \tag{12}$$

In large-signal (LS) conditions, the periodic working point is determined by the harmonic complex amplitudes of the various variables (voltages, currents, carrier concentrations etc.) evaluated at the harmonics $\omega_m = m\omega_0$ (m integer). In order to perform the perturbation analysis following the standard SSLS (or conversion) approach [5], [8], the frequency spectrum is conveniently decomposed into a superposition of nonoverlapping intervals denoted as *sidebands*. Each sideband is characterized by an absolute frequency ω_m^+ defined by an offset ω (called sideband angular frequency) with respect to the m-th harmonic ω_m; the absolute frequency within sideband m is therefore expressed as $\omega_m^+ = \omega_m + \omega$. The perturbation applied is an harmonic signal at sideband m, denoted as $(\tilde{v}_j)_m$; according to the small-change assumption, the resulting perturbation of the working point can be expressed (being affected by frequency conversion) as the superposition of harmonic components at all sidebands, e.g.,

$$n'_p(x,t) = n'_{p0}(x,t) + \sum_k \left(\tilde{n}'_p(x)\right)_k \exp(j\omega_k^+ t) \tag{13}$$

where $\left(\tilde{n}'_p\right)_k$ is the k-th sideband amplitude of the perturbation.

The k-th sideband amplitudes of the excess minority carrier densities satisfy the following equations, derived from (2)

$$j\omega_k^+\left(\tilde{n}'_p\right)_k = -\frac{\left(\tilde{n}'_p\right)_k}{\tau_n} + D_n\frac{d^2\left(\tilde{n}'_p\right)_k}{dx^2} \tag{14a}$$

$$j\omega_k^+(\tilde{p}'_n)_k = -\frac{(\tilde{p}'_n)_k}{\tau_p} + D_p\frac{d^2(\tilde{p}'_n)_k}{dx^2} \tag{14b}$$

completed by boundary conditions derived from (3)

$$\left(\tilde{n}'_p(-w_p)\right)_k = 0, \qquad (\tilde{p}'_n(w_n))_k = 0 \tag{15}$$

and from the linearization of (4) around the periodic working point. For instance, linearization of (4a) yields

$$\begin{aligned} n'_p(-x_p,t) \approx\, & n'_{p0}(-x_p,t) \\ & + n_{p,\rm eq}\exp\left(\frac{v_{j0}(t)}{V_T}\right)\frac{(\tilde{v}_j)_m\, e^{j\omega_m^+ t}}{V_T} \\ =\, & n'_{p0}(-x_p,t) \\ & + (\tilde{v}_j)_m\sum_l\left(\tilde{f}_n\right)_l\exp\left[j(\omega_l+\omega_m^+)t\right] \\ =\, & n'_{p0}(-x_p,t) \\ & + (\tilde{v}_j)_m\sum_k\left(\tilde{f}_n\right)_{k-m}\exp\left(j\omega_k^+ t\right) \end{aligned} \tag{16}$$

where $\left(\tilde{f}_n\right)_k$ is the kth harmonic component of the periodic function of time $f_n(t) = (n_{p,\rm eq}/V_T)\exp[v_{j0}(t)/V_T]$. A similar treatment is carried out for holes. This means that the boundary conditions of (14) are, in general, nonzero at all of the sideband frequencies (i.e., frequency conversion occurs), with sideband amplitudes

$$\left(\tilde{n}'_p(-x_p)\right)_k = (\tilde{f}_n)_{k-m}(\tilde{v}_j)_m \tag{17a}$$

$$(\tilde{p}'_n(x_n))_k = (\tilde{f}_p)_{k-m}(\tilde{v}_j)_m. \tag{17b}$$

After collecting the sideband amplitudes into a vector, (17) can be expressed in matrix form as

$$\tilde{\boldsymbol{n}}'_p(-x_p) = \tilde{\mathbf{F}}_n\cdot\tilde{\boldsymbol{v}}_j, \qquad \tilde{\boldsymbol{p}}'_n(x_n) = \tilde{\mathbf{F}}_p\cdot\tilde{\boldsymbol{v}}_j \tag{18}$$

where $\tilde{\mathbf{F}}$ is the conversion matrix [5], [8] associated to the linearized boundary conditions, with element (k,m) given by $\left(\tilde{\mathbf{F}}\right)_{k,m} = \left(\tilde{f}\right)_{k-m}$.

Finally, the sideband amplitudes of the perturbation of the intrinsic current are computed from (1) as

$$(\tilde{\imath})_k = qAD_n \frac{d\big(\tilde{n}'_p(x)\big)_k}{dx}\bigg|_{x=-x_p} - qAD_p \frac{d(\tilde{p}'_n(x))_k}{dx}\bigg|_{x=x_n}. \tag{19}$$

C. Noise Analysis

Noise analysis is based on the standard Green's function approach discussed, e.g., in [12], and will be carried out first in small-signal operation, deriving the stationary noise compact model, and then in forced, quasiperiodic large-signal conditions, where noise processes become cyclostationary [8]. In both cases, the noise model results from a two-step procedure. First, microscopic noise sources are identified within the device structure as a function of the noiseless working point (constant, or time-periodic). Secondly, noise sources are propagated to the device terminals to evaluate the device noise generators, by assuming that the related perturbation is small enough to allow for a linearized analysis. In this work, we shall consider only diffusion and generation-recombination (GR) noise mechanisms [12] in the neutral regions, and we shall completely neglect noise generated in the depletion region. In the first case, the microscopic noise source is a current density impressed into the continuity equation, while for GR noise the source is homogenous to the recombination rate: in both cases, the expressions for such sources depend only on the carrier concentrations evaluated in the noiseless device working point. More details can be found in [12].

Concerning the propagation of the microscopic noise sources, we have to evaluate, on the linearized model equations, a Green's function for each carrier species, namely $\tilde{G}_n$ and $\tilde{G}_p$. Considering short-circuit current noise generators, the output variable will be the current variation induced at the device anode (the p side ohmic contact) by an electron or hole scalar current injected into the electron or hole continuity equation, respectively.

For stationary noise evaluation, an SS analysis must be performed, i.e., the equations exploited for the determination of the Green's functions are (in the frequency domain) [12]

$$j\omega_{\rm SS}\tilde{n}'_p = -\frac{\tilde{n}'_p}{\tau_n} + D_n\frac{d^2\tilde{n}'_p}{dx^2} + \frac{\tilde{\imath}_n}{qA}\delta(x-x') \tag{20a}$$

$$j\omega_{\rm SS}\tilde{p}'_n = -\frac{\tilde{p}'_n}{\tau_p} + D_p\frac{d^2\tilde{p}'_n}{dx^2} - \frac{\tilde{\imath}_p}{qA}\delta(x-x') \tag{20b}$$

where the forcing term is an impulsive source, i.e., a Dirac's delta function in space, and $\tilde{\imath}$ is a scalar current injected in point x'. System (20) is completed by boundary conditions (10) and (see [12])

$$\tilde{n}'_p(-x_p) = 0, \qquad \tilde{p}'_n(x_n) = 0. \tag{21}$$

Concerning noise in LS operation, similar considerations apply (see Section V); the evaluation of the Green's functions requires an impulsive source term to be added for each sideband, thus leading to the equations

$$j\omega_k^+\big(\tilde{n}'_p\big)_k = -\frac{\big(\tilde{n}'_p\big)_k}{\tau_n} + D_n\frac{d^2\big(\tilde{n}'_p\big)_k}{dx^2} + \frac{(\tilde{\imath}_n)_k}{qA}\delta(x-x'), \tag{22a}$$

$$j\omega_k^+(\tilde{p}'_n)_k = -\frac{(\tilde{p}'_n)_k}{\tau_p} + D_p\frac{d^2(\tilde{p}'_n)_k}{dx^2} - \frac{(\tilde{\imath}_p)_k}{qA}\delta(x-x') \tag{22b}$$

with boundary conditions (15) and, in full analogy with (21)

$$\big(\tilde{n}'_p(-x_p)\big)_k = 0, \qquad (\tilde{p}'_n(x_n))_k = 0. \tag{23}$$

Notice that, in general, we should also evaluate the Green's functions for majority carriers: we will show in Section IV (the same result holds also for cyclostationary noise) that minority carriers suffice (see [2]) for evaluating the noise generator characteristics of the intrinsic diode.

III. Small-Signal and Conversion Compact Model

Following the discussion in Section II, both the SS and SSLS analyzes are carried out within a small-change approximation corresponding to a linearized set of boundary conditions.

A. Small-Signal Model

The solution of linear equations (9), completed by boundary conditions (10) and (11), is

$$\tilde{n}'_p(x) = \tilde{n}'_p(-x_p)\frac{\sinh\frac{w_p+x}{\tilde{L}_n}}{\sinh\frac{w_p-x_p}{\tilde{L}_n}} \tag{24a}$$

$$\tilde{p}'_n(x) = \tilde{p}'_n(x_n)\frac{\sinh\frac{w_n-x}{\tilde{L}_p}}{\sinh\frac{w_n-x_n}{\tilde{L}_p}} \tag{24b}$$

where $\tilde{L}_\alpha = L_\alpha/(a_\alpha + jb_\alpha)$ $(\alpha = n,p)$ is the frequency dependent diffusion length, and $a_\alpha + jb_\alpha = \sqrt{1+j\omega_{\rm SS}\tau_\alpha}$.

The intrinsic current perturbation $\tilde{\imath}$ is given by (12), and the device admittance is evaluated as $\tilde{y}(\omega_{\rm SS}) = \tilde{\imath}/\tilde{v}_j$

$$\tilde{y}(\omega_{\rm SS}) = \frac{qA}{V_T}\exp\left(\frac{v_{j0}}{V_T}\right)\sum_{\alpha=n,p}\frac{\alpha_{\overline{\alpha},\rm eq}D_\alpha}{\tilde{L}_\alpha}\coth\frac{w_{\overline{\alpha}}-x_{\overline{\alpha}}}{\tilde{L}_\alpha} \tag{25}$$

where $\overline{\alpha} = p,n$ for $\alpha = n,p$. This expression is the standard distributed model for the intrinsic diode SS admittance [1], [14].

B. Conversion (SSLS) Model

System (14), completed by boundary conditions (15) and (17), is formally identical to the SS equations, so that (24) are still valid for each sideband frequency

$$\left(\tilde{n}'_p(x)\right)_k = \left(\tilde{n}'_p(-x_p)\right)_k \frac{\sinh \frac{w_p+x}{\tilde{L}^+_{n,k}}}{\sinh \frac{w_p-x_p}{\tilde{L}^+_{n,k}}} \tag{26a}$$

$$\left(\tilde{p}'_n(x)\right)_k = \left(\tilde{p}'_n(x_n)\right)_k \frac{\sinh \frac{w_n-x}{\tilde{L}^+_{p,k}}}{\sinh \frac{w_n-x_n}{\tilde{L}^+_{p,k}}} \tag{26b}$$

where $\tilde{L}^+_{\alpha,k} = L_\alpha/(a^+_{\alpha,k} + jb^+_{\alpha,k})$, and $a^+_{\alpha,k} + jb^+_{\alpha,k} = \sqrt{1 + j\omega^+_k \tau_\alpha}$. Notice that frequency conversion takes place only through boundary condition (17).

Taking into account (19), (17) and defining the element (k,m) of the diode admittance conversion matrix as the ratio $(\tilde{i})_k/(\tilde{v}_j)_m$, the following result holds:

$$\left(\tilde{\mathbf{Y}}(\omega)\right)_{k,m} = qA \sum_{\alpha=n,p} \frac{D_\alpha (\tilde{f}_\alpha)_{k-m}}{\tilde{L}^+_{\alpha,k}} \coth \frac{w_{\overline{\alpha}} - x_{\overline{\alpha}}}{\tilde{L}^+_{\alpha,k}} \tag{27}$$

where $(\tilde{f}_\alpha)_k$ is the kth harmonic component of the periodic function of time $f_\alpha(t) = (\alpha_{\overline{\alpha},\mathrm{eq}}/V_T)\ \exp[v_{j0}(t)/V_T]$.

IV. Stationary Noise Compact Model

In SS conditions, noise is represented by stationary stochastic processes. As discussed in [12], the correlation spectrum of the current noise generator is expressed as the sum of the diffusion and GR spectra

$$S_i(\omega_{\mathrm{SS}}) = S_{i,D}(\omega_{\mathrm{SS}}) + S_{i,\mathrm{GR}}(\omega_{\mathrm{SS}}) \tag{28}$$

and the two contributions are

$$S_{i,D}(\omega_{\mathrm{SS}}) = A \sum_{\alpha=n,p} \int_\Omega K_{J_\alpha,J_\alpha}(x) \left| \frac{\partial \tilde{G}_\alpha}{\partial x} \right|^2 dx \tag{29}$$

$$S_{i,\mathrm{GR}}(\omega_{\mathrm{SS}}) = Aq^2 \sum_{\alpha,\beta=n,p} \int_\Omega K_{\gamma_\alpha,\gamma_\beta}(x) \tilde{G}_\alpha \tilde{G}^*_\beta dx \tag{30}$$

where the integration domain excludes the depletion region ($\Omega = \Omega_p \cup \Omega_n$ where $\Omega_p = [-w_p, -x_p]$ and $\Omega_n = [x_n, w_n]$), and K is the local noise source [12]

$$K_{J_n,J_n}(x) = 4q^2 n_0(x) D_n \tag{31a}$$

$$K_{J_p,J_p}(x) = 4q^2 p_0(x) D_p \tag{31b}$$

$$\begin{aligned} K_{\gamma_n,\gamma_n}(x) &= K_{\gamma_p,\gamma_p}(x) \\ &= -K_{\gamma_n,\gamma_p}(x). \end{aligned} \tag{32}$$

Let us consider first the electron Green's function $\tilde{G}_n = \tilde{i}_{\mathrm{cc},n}/\tilde{i}_n$. Assuming injection in $x' \in \Omega_p$ [see Fig. 3(a)] Kirchhoff current law (KCL) yields $\tilde{i}_{\mathrm{cc},n} + \tilde{i}_n - \tilde{i}_1 = 0$ where $\tilde{i}_1$ is given by the first term in (12). On the other hand, for $x' \in \Omega_n$, i.e., where electrons are majority carriers, all of the injected current flows through the ohmic contact in w_n and therefore $\tilde{i}_{\mathrm{cc},n} = 0$. Notice that this results from the assumption that the majority carriers are in equilibrium (low-injection approximation), and from considering the resistivity of the neutral side as negligible. The effect of the finite value of the resistivity can be taken into account in evaluating the Green's functions as discussed in Appendix A. Therefore

$$\begin{aligned} \tilde{G}_n(x') &= \frac{\tilde{i}_{\mathrm{cc},n}}{\tilde{i}_n} \\ &= \begin{cases} 0, & x' \in \Omega_n \\ -1 + \tilde{G}_{n_p}(x'), & x' \in \Omega_p, \end{cases} \end{aligned} \tag{33}$$

where $\tilde{G}_{n_p}(x') = \tilde{i}_1/\tilde{i}_n$.

The hole Green's function $\tilde{G}_p = \tilde{i}_{\mathrm{cc},p}/\tilde{i}_p$, defined in Fig. 3(b), is evaluated similarly. Assuming injection in $x' \in \Omega_p$, i.e., where holes are majority carriers, KCL reads $\tilde{i}_{\mathrm{cc},p} - \tilde{i}_p = 0$. For $x' \in \Omega_n$, $\tilde{i}_{\mathrm{cc},p} = \tilde{i}_2$ where $\tilde{i}_2$ is given by the second term in (12). This allows us to express

$$\begin{aligned} \tilde{G}_p(x') &= \frac{\tilde{i}_{\mathrm{cc},p}}{\tilde{i}_p} \\ &= \begin{cases} \tilde{G}_{p_n}(x'), & x' \in \Omega_n \\ 1, & x' \in \Omega_p \end{cases} \end{aligned} \tag{34}$$

where $\tilde{G}_{p_n}(x') = \tilde{i}_2/\tilde{i}_p$.

Because of (33) and (34), (29) reduces to

$$S_{i,D}(\omega_{\mathrm{SS}}) = A \sum_{\alpha=n,p} \int_{\Omega_{\overline{\alpha}}} K_{J_\alpha,J_\alpha}(x) \left| \frac{\partial \tilde{G}_{\alpha_{\overline{\alpha}}}}{\partial x} \right|^2 dx \tag{35}$$

i.e., diffusion noise in the diode is due only to velocity fluctuations of minority carriers in the two sides [2], [12]. Similarly, (32)–(34) allow to simplify (30) into

$$S_{i,\mathrm{GR}}(\omega_{\mathrm{SS}}) = Aq^2 \sum_{\alpha=n,p} \int_{\Omega_{\overline{\alpha}}} K_{\gamma_\alpha,\gamma_\alpha}(x) \left| \tilde{G}_{\alpha_{\overline{\alpha}}} \right|^2 dx. \tag{36}$$

The local noise sources for electrons in the p side are therefore

$$K_{J_n,J_n}(x) = 4q^2 n_{p0}(x) D_n \tag{37a}$$

$$K_{\gamma_n,\gamma_n}(x) = 2\frac{n_{p,\mathrm{eq}} + n_{p0}(x)}{\tau_n} \tag{37b}$$

with a similar expression for holes in the n side.

The noise contribution of majority carriers in the neutral sides correponds to the thermal noise of the series diode resistance, and can be added through embedding to the previous expressions (Fig. 2) in order to recover the total stationary noise spectrum.

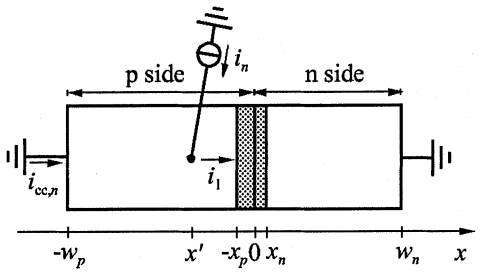

(a)

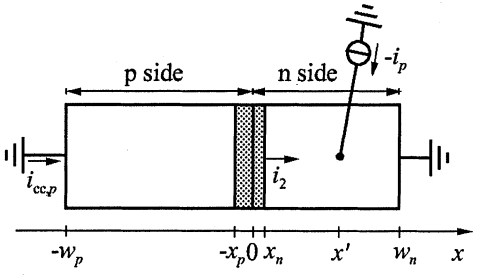

(b)

Fig. 3. Definition of short-circuit current Green's functions. (a) Electron Green's function. (b) Hole Green's function.

Following the results in Appendix B, the two relevant Green's functions are given by

$$\tilde{G}_{n_p}(x,\omega_{\rm SS}) = -\frac{\sinh\frac{w_p+x}{\tilde{L}_n}}{\sinh\frac{w_p-x_p}{\tilde{L}_n}}, \quad x\in\Omega_p \tag{38a}$$

$$\tilde{G}_{p_n}(x,\omega_{\rm SS}) = -\frac{\sinh\frac{w_n-x}{\tilde{L}_p}}{\sinh\frac{w_n-x_n}{\tilde{L}_p}}, \quad x\in\Omega_n. \tag{38b}$$

Making use of (5), (37) and (38), integrals in (35) and (36) can be easily evaluated, leading to the expression for the two contributions to the noise current spectrum in (39) and (40), shown at the bottom of the page, where $y_\alpha = (w_{\overline{\alpha}} - x_{\overline{\alpha}})/L_\alpha$, $g_n = n'_{p0}(-x_p)$, $g_p = p'_{n0}(x_n)$. Adding (39) and (40) yields the total noise current spectrum:

$$\begin{aligned} S_i(\omega_{\rm SS}) = {} & 2q^2A\sum_{\alpha=n,p}\frac{\frac{D_\alpha}{L_\alpha}}{\cosh(2a_\alpha y_\alpha)-\cos(2b_\alpha y_\alpha)} \\ & \times\Big\{ g_\alpha\left[2a_\alpha\sinh(2a_\alpha y_\alpha)\right. \\ & +2b_\alpha\sin(2b_\alpha y_\alpha)-\coth(y_\alpha) \\ & \times(\cosh(2a_\alpha y_\alpha)-\cos(2b_\alpha y_\alpha))] \\ & +2\alpha_{\overline{\alpha},\rm eq}\left[a_\alpha\sinh(2a_\alpha y_\alpha)\right. \\ & \left.+b_\alpha\sin(2b_\alpha y_\alpha)\right]\Big\}. \end{aligned} \tag{41}$$

A lengthy but straightforward calculation shows that (41) is equivalent to the standard relationship corresponding to the corrected shot-noise expression [2], [3]:

$$\begin{aligned} S_i(\omega_{\rm SS}) &= 4k_BT{\rm Re}\{\tilde{y}_{\rm SS}(\omega_{\rm SS})\} - 2qi_0 \\ &= 2q(i_0+2i_s) + 4k_BT \\ &\quad\times\left[{\rm Re}\{\tilde{y}_{\rm SS}(\omega_{\rm SS})\} - \tilde{y}_{\rm SS}(0)\right] \end{aligned} \tag{42}$$

where i_s is the diode reverse saturation current.

The frequency dependence of the two contributions (39) and (40) originates from the a and b parameters, and is therefore quite complex. As a general remark, the diffusion noise term (39) exhibits a constant spectrum up to frequencies of the order

$$\begin{aligned} S_{i,D}(\omega_{\rm SS}) = {} & 4q^2A\sum_{\alpha=n,p}\frac{D_\alpha}{L_\alpha}\frac{a_\alpha^2+b_\alpha^2}{\cosh(2a_\alpha y_\alpha)-\cos(2b_\alpha y_\alpha)} \\ & \times\Bigg\{\frac{g_\alpha}{\sinh(y_\alpha)}\left[\frac{\cosh(2a_\alpha y_\alpha)\cosh(y_\alpha)-1}{1-(2a_\alpha)^2}-\frac{2a_\alpha\sinh(2a_\alpha y_\alpha)\sinh(y_\alpha)}{1-(2a_\alpha)^2}\right. \\ & \left.+\frac{\cos(2b_\alpha y_\alpha)\cosh(y_\alpha)-1}{1-(2jb_\alpha)^2}+\frac{2b_\alpha\sin(2b_\alpha y_\alpha)\sinh(y_\alpha)}{1-(2jb_\alpha)^2}\right] \\ & +\alpha_{\overline{\alpha},\rm eq}\left[\frac{\sinh(2a_\alpha y_\alpha)}{2a_\alpha}+\frac{\sin(2b_\alpha y_\alpha)}{2b_\alpha}\right]\Bigg\} \end{aligned} \tag{39}$$

$$\begin{aligned} S_{i,\rm GR}(\omega_{\rm SS}) = {} & 2q^2A\sum_{\alpha=n,p}\frac{D_\alpha}{L_\alpha}\frac{1}{\cosh(2a_\alpha y_\alpha)-\cos(2b_\alpha y_\alpha)} \\ & \times\Bigg\{\frac{g_\alpha}{\sinh(y_\alpha)}\left[\frac{\cosh(2a_\alpha y_\alpha)\cosh(y_\alpha)-1}{1-(2a_\alpha)^2}-\frac{2a_\alpha\sinh(2a_\alpha y_\alpha)\sinh(y_\alpha)}{1-(2a_\alpha)^2}\right. \\ & \left.-\frac{\cos(2b_\alpha y_\alpha)\cosh(y_\alpha)-1}{1-(2jb_\alpha)^2}-\frac{2b_\alpha\sin(2b_\alpha y_\alpha)\sinh(y_\alpha)}{1-(2jb_\alpha)^2}\right] \\ & +2\alpha_{\overline{\alpha},\rm eq}\left[\frac{\sinh(2a_\alpha y_\alpha)}{2a_\alpha}-\frac{\sin(2b_\alpha y_\alpha)}{2b_\alpha}\right]\Bigg\} \end{aligned} \tag{40}$$

of the SS admittance corner frequency, where the noise current spectrum becomes an increasing function of frequency (see the discussion in [13]). GR noise contribution (40), on the other hand, shows the expected low-pass behavior, again with a corner frequency related to $\tilde{y}_{\rm SS}(\omega_{\rm SS})$, although not with an exactly lorentzian shape [13]. Notice that both diffusion and GR noise are needed to recover the shot-like expression (42), though for short side diodes the GR contribution becomes negligible with respect to the diffusion noise term.

V. Cyclostationary Noise Compact Model

In LS forced operation, noise is represented by cyclostationary stochastic processes, whose frequency components are correlated only if they are at the same distance from one of the harmonics of the working point [8], [12]; in other words, correlation takes place only between sidebands. For this reason, the statistical properties of such processes are represented by the so-called sideband correlation matrix (SCM) [8]. Also in this case, noise can be evaluated by means of a Green's function approach propagating the microscopic noise sources to the device terminals. Since the microscopic noise sources are modulated by the time-varying working point, they have to be modeled as cyclostationary processes characterized by their own SCM [6], [8]. Furthermore, the propagation step implies, as a matter of principle, frequency conversion. The Green's functions are therefore conversion operators, called conversion Green's functions (CGF) [8]. The element (k,m) of the CGF represents the output on sideband k induced by a unit impulse harmonic source term injected in sideband m. Notice that, since (22) and the boundary conditions (15), (23) are linear, injection in sideband m results into an output in sideband m only, i.e., no conversion effects actually take place: in other words, within the assumptions in our model the CGF's are diagonal.

With analogy to the discussion in Section IV, the short-circuit current noise SCM can be evaluated as

$$\left(\mathbf{S}_i(\omega)\right)_{k,m} = \left(\mathbf{S}_{i,D}(\omega)\right)_{k,m} + \left(\mathbf{S}_{i,\rm GR}(\omega)\right)_{k,m} \tag{43}$$

where the two contributions are

$$\left(\mathbf{S}_{i,D}(\omega)\right)_{k,m} = A \sum_{\alpha=n,p} \int_{\Omega_{\overline{\alpha}}} \left(\mathbf{K}_{J_\alpha,J_\alpha}(x)\right)_{k,m} \times \frac{\partial(\tilde{\mathbf{G}}_{\alpha_{\overline{\alpha}}})_{k,k}}{\partial x} \frac{\partial(\tilde{\mathbf{G}}^*_{\alpha_{\overline{\alpha}}})_{m,m}}{\partial x} dx \tag{44a}$$

$$\left(\mathbf{S}_{i,\rm GR}(\omega)\right)_{k,m} = Aq^2 \sum_{\alpha=n,p} \int_{\Omega_{\overline{\alpha}}} \left(\mathbf{K}_{\gamma_\alpha,\gamma_\alpha}(x)\right)_{k,m} \times (\tilde{\mathbf{G}}_{\alpha_{\overline{\alpha}}})_{k,k} (\tilde{\mathbf{G}}^*_{\alpha_{\overline{\alpha}}})_{m,m} dx. \tag{44b}$$

The local noise source for electrons in the p side is [8]

$$\left(\mathbf{K}_{J_n,J_n}(x)\right)_{k,m} = 4q^2 D_n \left[\left(\tilde{n}'_{p0}(x)\right)_{k-m} + n_{p,\rm eq}\delta_{k,m}\right] \tag{45a}$$

$$\left(\mathbf{K}_{\gamma_n,\gamma_n}(x)\right)_{k,m} = 2\frac{\left(\tilde{n}'_{p0}(x)\right)_{k-m} + n_{p,\rm eq}(1+\delta_{k,m})}{\tau_n} \tag{45b}$$

where $\delta_{k,m}$ is Kronecker's symbol. A similar expression holds for holes in the n side.

Concerning the Green's functions, inspection of (22), (15) and (23) allows (38) to be directly extended into

$$\left(\tilde{\mathbf{G}}_{n_p}(x,\omega)\right)_{k,k} = -\frac{\sinh\frac{w_p+x}{\tilde{L}^+_{n,k}}}{\sinh\frac{w_p-x_p}{\tilde{L}^+_{n,k}}}, \quad x\in\Omega_p \tag{46a}$$

$$\left(\tilde{\mathbf{G}}_{p_n}(x,\omega)\right)_{k,k} = -\frac{\sinh\frac{w_n-x}{\tilde{L}^+_{p,k}}}{\sinh\frac{w_n-x_n}{\tilde{L}^+_{p,k}}}, \quad x\in\Omega_n. \tag{46b}$$

Substituting (8), (45) and (46) into (44), and evaluating the resulting integrals, yields (47) and (48), shown at the bottom of the next page, where $\tilde{g}_{n,k} = \left(\tilde{n}'_{p0}(-x_p)\right)_k$, $\tilde{g}_{p,k} = \left(\tilde{p}'_{n0}(x_n)\right)_k$, and we have defined the following symbols:

$$\gamma^{(\alpha)}_{k+m} = a^+_{\alpha,k} + a^+_{\alpha,m} + j\left(b^+_{\alpha,k} - b^+_{\alpha,m}\right) \tag{49}$$

$$\gamma^{(\alpha)}_{k-m} = a^+_{\alpha,k} - a^+_{\alpha,m} + j\left(b^+_{\alpha,k} + b^+_{\alpha,m}\right) \tag{50}$$

$$\eta^{(\alpha)}_{k-m} = a_{\alpha,k-m} + jb_{\alpha,k-m}. \tag{51}$$

Finally, $A^{(\alpha)}_{k+m} = y_\alpha\gamma^{(\alpha)}_{k+m}$, $A^{(\alpha)}_{k-m} = y_\alpha\gamma^{(\alpha)}_{k-m}$, $B^{(\alpha)}_{k-m} = y_\alpha\eta^{(\alpha)}_{k-m}$.

Notice that the small-signal stationary noise spectrum can be obtained from the previous expressions by setting $k=m=0$ and $\omega=\omega_{\rm SS}$. In the case of a junction diode with long sides, (47) and (48) are significantly simplified, as shown in [11].

VI. Conclusions

A closed form, analytical compact model for the small-signal, conversion and noise behaviors of junction diodes has been presented. The model is based on decoupling the majority and minority carrier continuity equations in the neutral sides of the device, and therefore is based on the well known low-injection assumption. Noise analysis is carried out both in the small-signal case, wherein the well known corrected shot-like expression is derived, and in the case of forced large-signal periodic conditions, thus deriving a closed-form expression of the short-circuit current SCM. Furthermore, analytical expressions are also derived for the conversion device characteristics, i.e., for the diode admittance conversion matrix.

According to the model assumptions, the expressions are derived by neglecting the parasitic effect due to the (series) resistance of the neutral regions, which in turn is due to the resistivity associated to majority carrier conduction. The terminal values of the various quantities are recovered by applying well known circuit embedding techniques. Notice that, apart from the effect of the series resistance on the small-signal and conversion admittance parameters, thermal noise due to majority carriers in the neutral regions must also be taken into account for the terminal noise evaluation.

The model can also be considered as a starting point for the derivation of an analytical conversion and cyclostationary noise model for bipolar transistors, akin to the well known Ebers–Moll model for dc and small-signal analysis.

APPENDIX A
EFFECT OF R_S ON THE GREEN'S FUNCTIONS

The finite value of the resistivity of the neutral sides, besides being important for the junction admittance and noise spectra, has also an impact on the Green's functions exploited for the estimation of the device noise generators. While in the first case standard circuit embedding/deembedding techniques (based on the circuit in Fig. 2) can be used, the distributed nature of the Green's functions requires a careful discussion.

We discuss here the LS CGF's, since the SS case can be recovered by substituting the conversion matrices with the SS (scalar) parameters. For the sake of simplicity, we neglect the modulation of the neutral regions lengths due to the working point dependence of the depletion widths x_n, x_p (see Fig. 2), i.e., we assume $w_\alpha - x_\alpha \approx w_\alpha$. This means that we can decompose the total resistance R_s according to the contribution of the two sides $R_s = R_{sn} + R_{sp}$, both of them being constant resistances characterized by a diagonal conversion matrix [12]. Furthermore, a complete analysis requires to consider separately the case of injection of an electron or hole current into the n or p side: we shall explicitly treat the case of electron current injection only, since the extension to the other case is straightforward.

Let us consider first the injection of the impressed scalar electron current in the p side. We can represent the evaluation of the external CGF $\tilde{\mathbf{G}}_{ne}(x')$ for $x' \in \Omega_p$ according to the equivalent circuit shown in Fig. 4, where $i_{cc,ne}$ is the current induced at the terminal including the effect of R_s, and $R_{sp} = R_{sp1} + R_{sp2}$ with $R_{sp2} = R_{sp}|x'|/w_p$. The "inner" device is represented, after linearization, by the conversion matrix $\tilde{\mathbf{Y}}_j(\omega)$, that includes the parallel of the intrinsic conversion matrix (27) and of the conversion matrix derived by linearizing the junction capacitance expression around the working point [12]. Furthermore, we assume that the current variation induced at the boundary of the neutral region is given by the same expression exploited when the resistivity of the side is neglected: this is represented by the controlled current source in Fig. 4, which corresponds to current i_1 in Fig. 3 and contains the "intrinsic" CGF $\tilde{\mathbf{G}}_{n_p}$ as evaluated in Section V. Notice that, as already remarked, linear resistances are represented by diagonal conversion matrices of the type $R_{sp}\mathbf{I}$, where $\mathbf{I}$ is the identity matrix.

The external current sideband amplitudes $\tilde{i}_{cc,ne}$ satisfy

$$(\mathbf{I} + R_s\tilde{\mathbf{Y}}_j)\cdot\tilde{\boldsymbol{i}}_{cc,ne} = \tilde{\mathbf{G}}_{n_p}\cdot\tilde{\boldsymbol{i}}_n - (1 + R_{sp2} + R_{sn})\tilde{\boldsymbol{i}}_n, \quad (52)$$

therefore the "intrinsic" CGF $\tilde{\mathbf{G}}_{n_p}(x')$ is related to the external CGF $\tilde{\mathbf{G}}_{ne}(x')$, corresponding to $\tilde{i}_{cc,ne}$, by means of the linear transformation (where $x' \in \Omega_p$)

$$\tilde{\mathbf{G}}_{n_p}(x') = (\mathbf{I} + R_s\tilde{\mathbf{Y}}_j)\cdot\tilde{\mathbf{G}}_{ne} + [R_{sp2}(x') + R_{sn}]\tilde{\mathbf{Y}}_j + \mathbf{I}. \quad (53)$$

$$\begin{aligned}(\mathbf{S}(\omega)_{i,D})_{k,m} = {} & 4q^2A\sum_{\alpha=n,p}\frac{D_\alpha}{L_\alpha}\frac{(a^+_{\alpha,k} + jb^+_{\alpha,k})(a^+_{\alpha,m} - jb^+_{\alpha,m})}{\cosh A^{(\alpha)}_{k+m} - \cosh A^{(\alpha)}_{k-m}} \\ & \times\left\{\frac{(\tilde{g}_\alpha)_{k-m}}{\sinh B^{(\alpha)}_{k-m}}\left[\frac{\eta^{(\alpha)}_{k-m}\left[\cosh B^{(\alpha)}_{k-m}\cosh A^{(\alpha)}_{k+m} - 1\right]}{\left(\eta^{(\alpha)}_{k-m}\right)^2 - \left(\gamma^{(\alpha)}_{k+m}\right)^2}\right.\right. \\ & -\frac{\gamma^{(\alpha)}_{k+m}\sinh B^{(\alpha)}_{k-m}\sinh A^{(\alpha)}_{k+m}}{\left(\eta^{(\alpha)}_{k-m}\right)^2 - \left(\gamma^{(\alpha)}_{k+m}\right)^2} + \frac{\eta^{(\alpha)}_{k-m}\left[\cosh B^{(\alpha)}_{k-m}\cosh A^{(\alpha)}_{k-m} - 1\right]}{\left(\eta^{(\alpha)}_{k-m}\right)^2 - \left(\gamma^{(\alpha)}_{k-m}\right)^2} \\ & \left.\left.-\frac{\gamma^{(\alpha)}_{k-m}\sinh B^{(\alpha)}_{k-m}\sinh A^{(\alpha)}_{k-m}}{\left(\eta^{(\alpha)}_{k-m}\right)^2 - \left(\gamma^{(\alpha)}_{k-m}\right)^2}\right] + \alpha_{\overline{\alpha},\mathrm{eq}}\delta_{k,m}\left[\frac{\sinh A^{(\alpha)}_{k+m}}{\gamma^{(\alpha)}_{k+m}} + \frac{\sinh A^{(\alpha)}_{k-m}}{\gamma^{(\alpha)}_{k-m}}\right]\right\}\end{aligned} \quad (47)$$

$$\begin{aligned}(\mathbf{S}(\omega)_{i,\mathrm{GR}})_{k,m} = {} & 2q^2A\sum_{\alpha=n,p}\frac{\frac{D_\alpha}{L_\alpha}}{\cosh A^{(\alpha)}_{k+m} - \cosh A^{(\alpha)}_{k-m}} \\ & \times\left\{\frac{(\tilde{g}_\alpha)_{k-m}}{\sinh B^{(\alpha)}_{k-m}}\left[\frac{\eta^{(\alpha)}_{k-m}\left[\cosh B^{(\alpha)}_{k-m}\cosh A^{(\alpha)}_{k+m} - 1\right]}{\left(\eta^{(\alpha)}_{k-m}\right)^2 - \left(\gamma^{(\alpha)}_{k+m}\right)^2}\right.\right. \\ & -\frac{\gamma^{(\alpha)}_{k+m}\sinh B^{(\alpha)}_{k-m}\sinh A^{(\alpha)}_{k+m}}{\left(\eta^{(\alpha)}_{k-m}\right)^2 - \left(\gamma^{(\alpha)}_{k+m}\right)^2} - \frac{\eta^{(\alpha)}_{k-m}\left[\cosh B^{(\alpha)}_{k-m}\cosh A^{(\alpha)}_{k-m} - 1\right]}{\left(\eta^{(\alpha)}_{k-m}\right)^2 - \left(\gamma^{(\alpha)}_{k-m}\right)^2} \\ & \left.\left.+\frac{\gamma^{(\alpha)}_{k-m}\sinh B^{(\alpha)}_{k-m}\sinh A^{(\alpha)}_{k-m}}{\left(\eta^{(\alpha)}_{k-m}\right)^2 - \left(\gamma^{(\alpha)}_{k-m}\right)^2}\right] + \alpha_{\overline{\alpha},\mathrm{eq}}(1+\delta_{k,m})\left[\frac{\sinh A^{(\alpha)}_{k+m}}{\gamma^{(\alpha)}_{k+m}} - \frac{\sinh A^{(\alpha)}_{k-m}}{\gamma^{(\alpha)}_{k-m}}\right]\right\}\end{aligned} \quad (48)$$

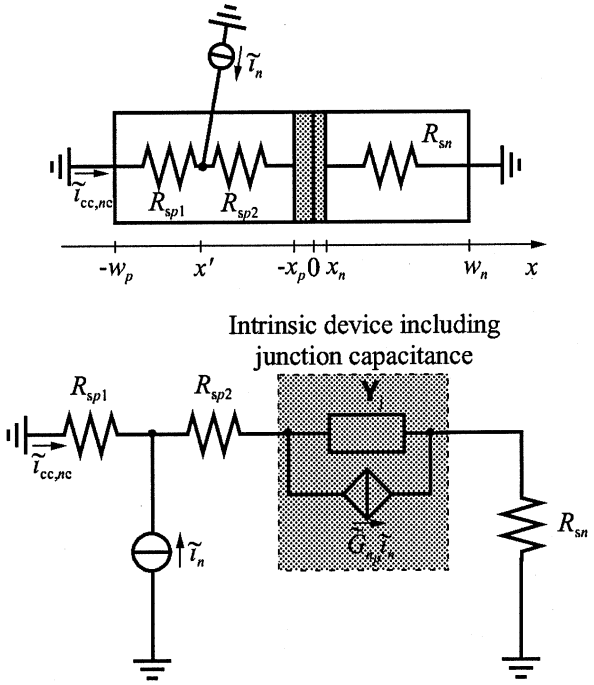

Fig. 4. Equivalent circuit representing the evaluation of the electron CGF including the effect of the resisitivity of the neutral sides: injection in the p side.

Notice that, for $R_s = 0$, the previous expression reduces to the relationship (33) discussed in Section IV.

On the other hand, considering electron current injection in the n side ($\tilde{\mathbf{G}}_{n,e}(x')$ for $x' \in \Omega_n$) leads to the the equivalent circuit shown in Fig. 5, where again we have assumed that the current variation induced at the border of the neutral region has the same value as for null resisitivity, i.e., zero [see (33)]. Notice that in Fig. 5 $R_{sn} = R_{sn1} + R_{sn2}$, with $R_{sn2} = R_{sn}(1 - x'/w_n)$.

The external current sideband amplitudes $\tilde{\imath}_{\mathrm{cc},ne}$ satisfy in this case

$$(\mathbf{I} + R_s \tilde{\mathbf{Y}}_j) \cdot \tilde{\boldsymbol{\imath}}_{\mathrm{cc},ne} = -R_{sn2} \tilde{\boldsymbol{\imath}}_n \tag{54}$$

therefore the external CGF $\tilde{\mathbf{G}}_{ne}(x')$ for $x' \in \Omega_n$ is given by

$$\tilde{\mathbf{G}}_{ne}(x') = R_{sn2}(x')(\mathbf{I} + R_s \tilde{\mathbf{Y}}_j)^{-1} \cdot \tilde{\mathbf{Y}}_j. \tag{55}$$

Appendix B
SS Green's Functions Evaluation

The Green's functions to be exploited for small-signal noise analysis are defined by continuity equations (20). For example, (20a) can be solved separately for $x < x'$ and $x > x'$, where the differential equation is homogeneous. The two solutions must satisfy boundary conditions (10), (21), and the jump condition [12]

$$\left.\frac{\partial \tilde{n}'_p}{\partial x}\right|_{x=x'+} = \left.\frac{\partial \tilde{n}'_p}{\partial x}\right|_{x=x'-} - \frac{\tilde{\imath}_n}{qAD_n}. \tag{56}$$

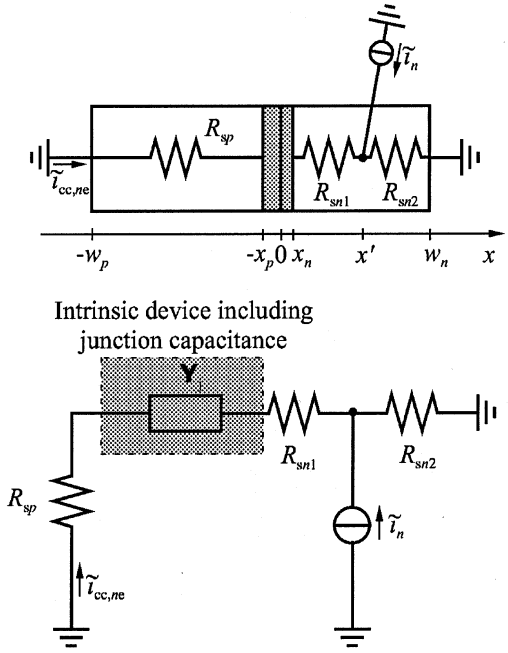

Fig. 5. Equivalent circuit representing the evaluation of the electron CGF including the effect of the resisitivity of the neutral sides: injection in the n side.

Straightforward calculations lead to

$$\tilde{n}'_p = -\frac{\tilde{L}_n \tilde{\imath}_n}{qAD_n} \begin{cases} \dfrac{\sinh\frac{w_p+x}{\tilde{L}_n}\sinh\frac{x'+x_p}{\tilde{L}_n}}{\sinh\frac{w_p-x_p}{\tilde{L}_n}}, & -w_p \le x \le x' \\ \dfrac{\sinh\frac{w_p+x'}{\tilde{L}_n}\sinh\frac{x+x_p}{\tilde{L}_n}}{\sinh\frac{w_p-x_p}{\tilde{L}_n}}, & x' \le x \le -x_p \end{cases} \tag{57}$$

and the corresponding short-circuit current induced at the device terminal is given by the first term in (12)

$$\tilde{\imath}_1 = qAD_n \left.\frac{d\tilde{n}'_p}{dx}\right|_{x=-x_p}. \tag{58}$$

A similar treatment for holes in the n side, based on the solution of (20b), leads to

$$\tilde{p}'_n = \frac{\tilde{L}_p \tilde{\imath}_p}{qAD_p} \begin{cases} \dfrac{\sinh\frac{w_n-x'}{\tilde{L}_p}\sinh\frac{x-x_n}{\tilde{L}_p}}{\sinh\frac{w_n-x_n}{\tilde{L}_p}}, & x_n \le x \le x' \\ \dfrac{\sinh\frac{x'-x_n}{\tilde{L}_p}\sinh\frac{w_n-x}{\tilde{L}_p}}{\sinh\frac{w_n-x_n}{\tilde{L}_p}}, & x' \le x \le w_n \end{cases} \tag{59}$$

and

$$\tilde{\imath}_2 = -qAD_p \left.\frac{d\tilde{p}'_n}{dx}\right|_{x=x_n}. \tag{60}$$

Since the Green's functions are defined as $\tilde{G}_{n_p} = \tilde{\imath}_1/\tilde{\imath}_n$ and $\tilde{G}_{p_n} = \tilde{\imath}_2/\tilde{\imath}_p$, (58) and (60) yield (38).

References

[1] W. Shockley, *Electrons and Holes in Semiconductors*. Princeton, NJ: Van Nostrand, 1950.

[2] K. M. van Vliet, "General transport theory of noise in pn–junction-like devices—I: Three-dimensional green's function formulation," *Solid State Electron*, vol. 15, pp. 1033–1053, 1972.
[3] A. van der Ziel, *Noise in Solid-State Devices And Circuits*. New York: Wiley, 1986.
[4] C. Dragone, "Analysis of thermal and shot noise in pumped resistive diodes," *Bell Syst. Tech. J.*, vol. 47, pp. 1883–1902, 1968.
[5] S. Maas, *Nonlinear Microwave Circuits*. Norwood, MA: Artech House, 1988.
[6] F. Bonani, S. Donati Guerrieri, and G. Ghione, "Noise source modeling for cyclostationary noise analysis in large-signal device operation," *IEEE Trans. Electron Devices*, vol. 49, pp. 1640–1647, Sept. 2002.
[7] ——, "Physics-based simulation techniques for small- and large-signal device noise analysis in RF applications," *IEEE Trans. Electron Devices*, vol. 50, pp. 633–644, Mar. 2003.
[8] F. Bonani, S. Donati Guerrieri, G. Ghione, and M. Pirola, "A TCAD approach to the physics-based modeling of frequency conversion and noise in semiconductor devices under large-signal forced operation," *IEEE Trans. Electron Devices*, vol. 48, pp. 966–977, May 2001.
[9] J. E. Sanchez, G. Bosman, and M. E. Law, "Two-dimensional semiconductor device simulation of trap-assisted generation-recombination noise under periodic large-signal conditions and its use for developing cyclostationary circuit simulation models," *IEEE Trans. Electron Devices*, vol. 50, pp. 1353–1362, May 2003.
[10] F. Danneville, G. Dambrine, and A. Cappy, "Noise modeling in MESFET and HEMT mixers using a uniform noisy line model," *IEEE Trans. Electron Devices*, vol. 45, pp. 2207–2212, Oct. 1998.
[11] F. Bonani, S. Donati Guerrieri, and G. Ghione, "A new, closed-form compact model for the cyclostationary noise and LS conversion behavior of RF junction diodes," in *IEDM Tech. Dig.*, San Francisco, CA, Dec. 8–11, 2002, pp. 137–140.
[12] F. Bonani and G. Ghione, *Noise in Semiconductor Devices: Modeling and Simulation–Springer Series in Advanced Microelectronics*. Berlin, Germany: Springer Verlag, 2001.
[13] F. Bonani, S. Donati Guerrieri, and G. Ghione, "Compact conversion and cyclostationary noise modeling of pn–junction diodes in low-injection—Part II: Discussion," *IEEE Trans. Electron Devices*, vol. 51, pp. 477–485, Mar. 2004.
[14] S. M. Sze, *Physics of Semiconductor Devices*, 2 ed. New York: Wiley, 1981.
[15] R. B. Darling, "A full dynamic model for pn-junction diode switching transients," *IEEE Trans. Electron Devices*, vol. 42, pp. 969–976, May 1995.

Fabrizio Bonani (S'89–M'91–SM'02) was born in Torino, Italy, in 1967. He received the Laurea degree (*cum laude*) and the Ph.D. degree in electronic engineering from Politecnico di Torino, in 1992 and 1996, respectively.

Since 1995, he has been with the Electronics Department, Politecnico di Torino, first as a Researcher and since 2001, as an Associate Professor of electronics. His research interests are mainly devoted to the physics-based simulation of semiconductor devices, with special emphasis on the noise analysis of microwave field-effect and bipolar transistors, and to the thermal analysis of power microwave circuits. Part of his research concerns the analysis and simulation of nonlinear dynamical systems. From 1994 to 1995, he was with the ULSI Technology Research Department, Bell Laboratories, Murray Hill, NJ, as a consultant, working on physics-based noise modeling of electron devices.

Simona Donati Guerrieri (M'97) was born in 1969 in Milan, Italy. She received the degree in theoretical physics from the University of Milan, in 1993 and the Ph.D. degree in electron devices from University of Trento, Trento, Italy, in 1999.

She is presently working as a Researcher in the Electronics Department, Politecnico of Torino, Torino, Italy, where she joined the microwave electronics group. Her research interests include the modeling and simulation of microwave solid-state devices, including physics-based noise analysis, and the RF and microwave integrated circuit design.

Giovanni Ghione (M'87–SM'94) was born in 1956 in Alessandria, Italy. He received the degree (*cum laude*) in electronic engineering from Politecnico di Torino, Torino, Italy, in 1981.

In 1983 he became a Research Assistant with Politecnico di Torino and from 1987 to 1990 an Associate Professor with Politecnico di Milano, Milan, Italy. In 1990, he joined the University of Catania, Catania, Italy, as Full Professor of electronics, and since 1991, he has held the same position in the Faculty of Engineering, Politecnico di Torino. Since 1981, he has been engaged in Italian and European research projects (ESPRIT 255, COSMIC, and MANPOWER) in the field of active and passive microwave computer-aided design. His present research interests concern the physics-based simulation of active microwave and optoelectronic devices, with particular attention to noise modeling, thermal modeling, and active device optimization. His research interests also include several topics in computational electromagnetics, including coplanar component analysis. He has published more than 200 papers and book chapters and four books in the above fields.

Prof. Ghione is a member of the Associazione Elettrotecnica Italiana and a member of the Editorial Board of the IEEE TRANSACTIONS ON MICROWAVE THEORY AND TECHNIQUES.